Journal of Inorganic and General Chemistry
ZAAC
Zeitschrift für anorganische und allgemeine Chemie
www.zaac.wiley-vch.de
RESEARCH ARTICLE
DOI: 10.1002/zaac.202400064

Structural Study on Alkali-Carboxylate Functionalized Late-Transition Metal Bis(dithiocarbamate) Complexes

Phil Liebing,*[a, b] Vreni Behling,[a] and Juliane Witzorke[b]

Dedicated to Professor Frank T. Edelmann on the occasion of his 70th birthday

Lithium, sodium, and potassium derivatives of amino-acid derived bis(dithiocarbamate) complexes of bivalent nickel, palladium, platinum, and copper are readily available by treatment of the carboxylic-acid functionalized complexes with the respective alkali metal hydroxide. Representative derivatives of the types $A_4[M(L1)_2]$, $A_2[M(HL1)_2]$, $A[M(HL1)(H_2L1)]$ (*N*-dithioato-iminodiacetate, L1), and $A_2[M(L2,3)_2]$ (*N*-dithioato-L-prolinate, L2, and -*N*-benzylglycinate, L3; A=Li, Na, K; M=Ni, Pd, Pt, Cu) were isolated and characterized by spectroscopic and thermal methods. Six entries were accessible to single-crystal X-ray structure determination, revealing the presence of different coordination-polymeric structures and hydrogen-bonded assemblies comprising solvent-separated cations in the solid state. While the transition metal always retains its all-sulfur coordination with defined geometry, the alkali metals are structurally more flexible. The latter are usually coordinated by carboxylate and water, but additional interactions with sulfur donors are also relevant in some cases.

Introduction

Transition metal complexes with dithiocarbamate ligands derived from aminocarboxylic acids (AA-DTCs) have widely been investigated due to their biological activity. Particular attention have gained complexes of the types $Mn(AA\text{-}dtc)(CO)_4$ (CO-releasing molecules),[1] $TcN(AA\text{-}dtc)_2$ (radiopharmaceuticals),[2] $Fe(AA\text{-}dtc)_3$ and related species (NO spin traps for EPR imaging),[3] $M(AA\text{-}dtc)_2$ (M=Pd, Pt) and related heteroleptic complexes (anticancer agents),[4–6] $Cu(AA\text{-}dtc)_2$ (various potential applications due to their redox activity),[7,8–11] and $AuX_2(AA\text{-}dtc)$ (X=Cl, Br; anticancer agents).[6,8,12] For such applications, the carboxylic-acid functional groups are deprotonated in situ by dissolving in buffered aqueous solutions at physiological pH, or esterified derivatives are used in order to optimize the biodistribution of the molecules by varying their hydrophilicity/lipophilicity profile. Apart from biomedical applications, AA-DTC ligands represent ditopic S,O-ligands that are well suited for the targeted preparation of heterobimetallic coordination compounds (Scheme 1). In their homoleptic AA-DTC complexes, Co^{3+},[13–17] Ni^{2+},[13,14,16,18–21] Pd^{2+},[21,22] Pt^{2+},[17,23,24] Cu^{2+},[9,13,14,16,21,25] or Au^{3+}[25–27] are coordinated highly selectively by the DTC group in a κ^2S,S' mode. In a second step, the so formed dithiocarbamato-carboxylate (DTCC) metalloligand can be transformed into a heterobimetallic product by salt-metathesis using an alkali carboxylate derivative,[16,24] or by metalating the free carboxylic acid by reaction with a metal hydroxide or acetate.[24,25,28,29] In the target products, divalent platinum retains its sulfur coordination even in combination with another rather thiophilic metal ion such as Cd^{2+},[29] whereas Ni^{2+}[28,29] and Cu^{2+}[25,29] as well as organotin(IV) moieties[30] are more flexible and can be coordinated either by the sulfur donors or by the oxygen donors depending on the softness of the competing metal component.

X-ray crystallographic structure elucidation has shown that alkaline earth metal compounds display rather ionic structures depending on the Lewis acidity of the metal, including salt-like structures with separated $[Mg(H_2O)_6]^{2+}$ ions for magnesium[29] and densely packed networks with alkaline-earth metal atoms irregularly coordinated by carboxylate and water donors for strontium and barium.[16,25,29] By contrast, bidentate transition metals with a preferred regular six- or five-coordination give more regular assemblies. Zn/Pt derivatives form linear polymeric chains with monocarboxylate ligands derived from sarcosine or L-proline.[24] Two-dimensional arrays of different porosity have been obtained with the iminodiacetic acid-derived dicarboxylate ligand $\{SSCN(CH_2COO)_2\}^{3-}$ (=L1), applying the hard/soft metal combinations Zn/Ni and Zn/Pd,[28] Zn/Pt,[24] as well as Fe/Pt, Co/Pt, Ni/Pt, and Cd/Pt.[29] While the Ni, Pd, and Pt metalloligands $[M(H_2L1)_2]$ (M=Ni–Pt) or $[M(L1)_2]^{4-}$, respectively, contribute very similarly to structures and properties (square-planar, diamagnetic complexes), the Cu analog was shown to be structurally more diverse as it can form assemblies with coordination numbers larger than four through additional Cu···S contacts.[25] As compared to heterobimetallic AA-DTCs

[a] Dr. P. Liebing, V. Behling
Institute of Inorganic and Analytical Chemistry
Friedrich Schiller University Jena
Humboldtstr. 8, 07743 Jena, Germany
E-mail: phil.liebing@uni-jena.de
[b] Dr. P. Liebing, J. Witzorke
Institute of Chemistry
Otto von Guericke University Magdeburg
Universitätsplatz 2, 39106 Magdeburg, Germany

Supporting information for this article is available on the WWW under https://doi.org/10.1002/zaac.202400064

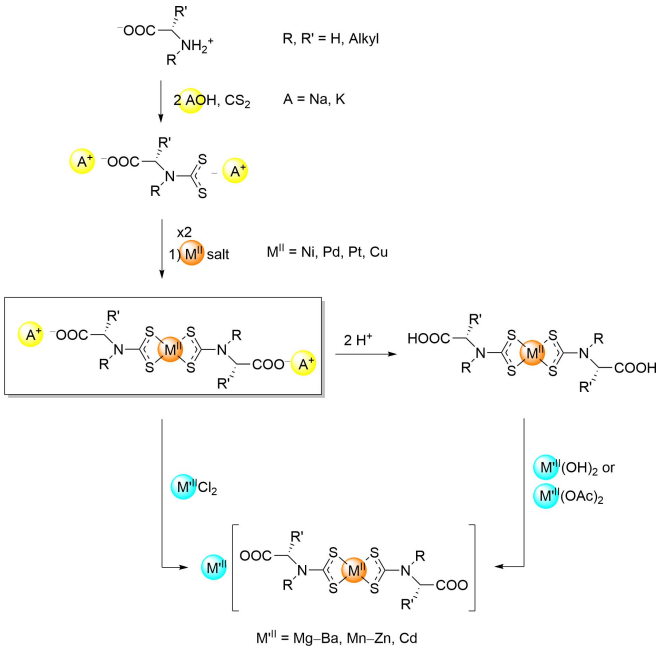

Scheme 1. General scheme for the synthesis of homo- and heterometallic transition-metal bis(dithiocarbamate) complexes derived from α-amino acids, illustrating the corresponding alkali-carboxylate functionalized complexes (framed entry) as important synthetic intermediates.[16,24,25,28,29]

with divalent oxophilic metals, related compounds with monovalent metals as the oxophilic component are less studied. $Na_4[Ni(L1)_2]$ (**14-Na**) and $Na_4[Cu(L1)_2]$ (**17-Na**) have been synthesized by ligand exchange from Na_3L1 (**1-Na**) and $[Ni(NH_3)_6]Cl_2$ or $[Cu(NH_3)_4]Cl_2$, respectively, and both products have been characterized only by elemental analyses and UV/Vis spectroscopy.[16] For the sake of investigating their biological activity, sodium and potassium salts of different palladium bis(AA-DTC) complexes were synthesized in one-pot reactions from the amino acid and potassium hydroxide, or amino-acid sodium salt, with CS_2 and $PdCl_2$. For these complexes the separation from the alkali chloride by-product is not documented, and only some entries have been characterized by thermal and spectroscopic methods.[31] In several other studies where late-transition metal AA-DTC complexes were subjected to biomedical studies, the solubility of the complexes under physiological conditions is more relevant than the specific nature of the peripheral oxygen groups, so that it is very likely that they exist in the form of their sodium or potassium carboxylate salts in solution.[4,10,11,27] In our previous studies using isolated, protonated AA-DTC complexes, the potassium carboxylate derivatives appeared as intermediates during the synthesis of the respective complexes from the respective alkali metal AA-DTCs, prior to protonation of the carboxylate group(s).[24,25,28,29] In view of their synthetic importance and the lack of knowledge about their properties and solid-state structures, we were interested in the full characterization of alkali metal derivatives of different group-10 and group-11 bis(AA-DTC) complexes. We report here the synthesis and full characterization of representative entries of Li, Na, and K compounds of different AA-DTC complexes derived from iminodiacetic acid (L1), L-proline (L2), and *N*-benzylglycine (L3; Scheme 2), including X-ray single-crystal structure determination of several compounds.

Results and Discussion

Synthetic strategy and characterization of new precursor complexes 11–13. The respective bis(dithiocarbamate) complexes of Ni^{2+}, Pd^{2+}, Pt^{2+}, and Cu^{2+} ions with the AA-DTC ligands shown in Scheme 2 form cleanly when a suitable metal chloride precursor is allowed to react with isolated or *in-situ* generated alkali metal AA-DTC salt in aqueous solution. An initial screening with the attempt to isolate the alkali metal salts of the complexes directly from the reaction mixture led to rather unsatisfactory results, because most of the alkali metal salts appeared to be very soluble in water and therefore hardly separable from the chloride salt by-product ACl (A=Li, Na, K). Consequently, we decided to prepare the target compounds by metalation of the carboxylic acid derivatives **4–13** with defined equivalents of LiOH, NaOH, or KOH (Scheme 3). Among them, compounds **11–13** comprising the *N*-benzlglycine derived

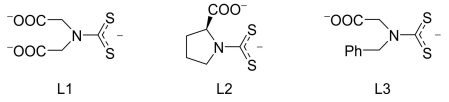

Scheme 2. Amino-acid dithiocarbamate ligands used in this study: *N*-dithioato-iminodiacetate (L1; **1**), –L-prolinate (L2; **2**), and –*N*-benzylglycinate (L3; **3**).

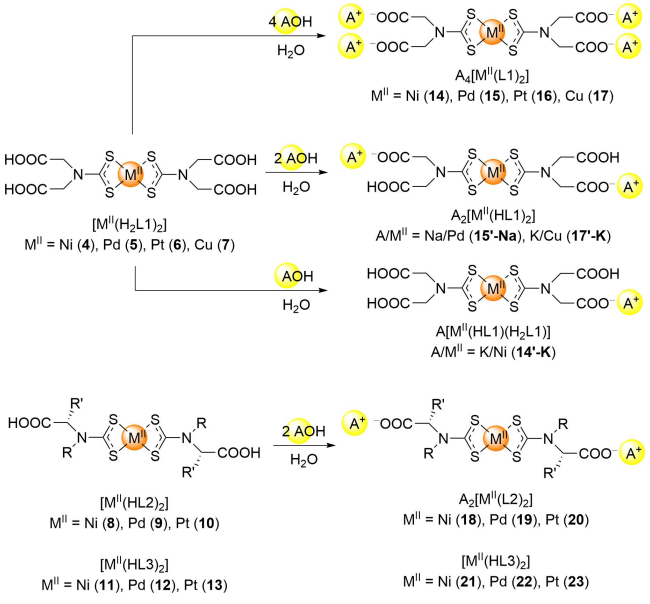

Scheme 3. Synthesis of the target compounds **14–23** by metalation of the parent carboxylic acid derivatives **4–13** with alkali metal hydroxides.

ligand L3 have not been reported previously, and consequently we provide the full characterization data herein. Like the homologous series **4–6**, the ^{1}H and ^{13}C NMR spectra are virtually identical with the exception of the *C*SS signal which shifts significantly downfield in going from Ni to Pd to Pt. The ^{13}C chemical shifts are similar to those for **4–6**,[24,28] showing that the benzyl groups do not exert a notable influence on the electronic structure of the $M(DTC)_2$ core. All three compounds do not melt without decomposition; the decomposition temperature of the Ni complex **11** under nitrogen (230 °C) is significantly higher than for the related **4** (217 °C),[28] whereas the T_{Dec} values of the Pd complexes **12** (253 °C) and **5** (248 °C)[28] deviate less. The identity of the complexes was also confirmed by ESI mass spectrometry, as the molecule in the form of an Na^+ adduct or in singly deprotonated state was detected in each case. Furthermore, the molecular structure of the nickel complex **11** was determined by single-crystal X-ray diffraction of a crystalline solvate with one equiv. DMSO (see Figure S12). The two CH_2COOH residues are in a *syn*-configuration, which is rather unusual as the vast majority of $Ni(DTC)_2$ complexes with asymmetric DTC ligands deposited in the Cambridge Structural Database (CSD)[32] possesses crystallographically imposed inversion symmetry, being compatible only with an *anti*-arrangement of the substituents. The lack of inversion symmetry leads to a marginal deviation of the $Ni(DTC)_2$ core from planarity in **11** · DMSO (angle between NiS_2 planes 1.89(3)°). Nonetheless, the Ni–S bond lengths are in a narrow range of 218.80(8)–220.42(7) pm, which resembles the values observed for other nickel bis(DTC) complexes deposited in the CSD (218.4–221.6 pm for > 95 % of the available data).

Preparation of alkali metal compounds 14–23. All carboxylic-acid functionalized complexes dissolve cleanly in water upon addition of the equivalent amount of alkali metal hydroxide required for deprotonation of all COOH groups. Many of the target products could be isolated from the aqueous solution in good yields by precipitation with acetone (Table 1). For a representative series of Na/Ni compounds derived from different amino acids, the solubility in acetone/water mixtures (v:v 5:2) correlates well with the polarity of the ligand backbone: $Na_4[Ni(L1)_2]$ (**14-Na**) < $Na_2[Ni(L2)_2]$ (**18-Na**) < $Na_2[Ni(L3)_2]$ (**21-Na**). The high solubility of **21-Na** made it necessary to evaporate the aqueous solution prior to addition of acetone, since the product did not precipitate from acetone/water even at −25 °C. However, the compound is virtually insoluble in pure acetone, as observed for all other sodium salts. Notably, once isolated as a solid, **21-Na** does also not dissolve in water. For entry **14-Na**, both the alkali metal and the transition metal were varied in order to study their influence on the product properties. The preparation of $Na_4[Pd(L1)_2]$ (**15-Na**), $Na_4[Pt(L1)_2]$ (**16-Na**), and $Na_4[Cu(L1)_2]$ (**17-Na**) was performed similarly as for their Ni analog and afforded products of comparable solubility properties. By contrast, $Li_4[Ni(L1)_2]$ (**14-Li**) and $K_4[Ni(L1)_2]$ (**14-K**) appeared to be much more soluble in water/acetone than **14-Na**, so that isolation required evaporation of the aqueous solution to dryness. While **14-Li** forms an insoluble acetone solvate of the approximate composition **14-Li** ·4 H_2O·0.67 acetone, **14-K** was isolated as a monohydrate, which is soluble even in pure acetone to some extent. Hydrated solid products were also obtained for **18-Na** and **21-Na**; the respective water contents were determined by elemental analyses and thermal analysis (see Table S1). Finally, it was found that the partially protonated derivatives $K[Ni(HL1)(H_2L1)]$ (**14′-K**) and $K_2[Cu(HL1)_2]$ (**17′-K**) could also be prepared in a straightforward manner, as they are much less soluble than the respective fully metalated target products and precipitate directly from aqueous solution. This finding can probably be explained with the circumstance that the relatively soft K^+ ion fits better with lowly charged $[M(HL1)(H_2L)_2]^-$ or $[M(HL1)_2]^{2-}$ counterions in terms of lattice energy than with $[M(L1)_2]^{4-}$; a similar behavior is known for e.g. the alkali carbonates and hydrogen carbonates ($NaHCO_3$ is more water soluble than Na_2CO_3, whereas $KHCO_3$ is less soluble than K_2CO_3).[33]

Spectroscopic characterization. All isolated products are non-hygroscopic, bench-stable solids, which were characterized by standard analytical techniques. The metalation of the carboxylic-acid functionalities can easily be monitored by a) shift of the ν(C=O) bands by ca. 130–200 cm^{-1} in the IR spectrum to smaller wavenumbers (see Figures S2–S6), and b) downfield shift of the *C*OO signal by about 4–6 ppm in the ^{13}C NMR spectrum (Table 2). The IR data show that the deprotonation of the COOH groups seems to have no significant influence on the $M(DTC)_2$ core, as the ν(M–S) band positions remain almost unchanged upon metalation. However, the chemical shift of the ^{13}C NMR signal of the *C*SS signal

Table 1. Isolated yields (not optimized) and temperatures of degradation of the $M(DTC)_2$ core (T_{Dec}) for the isolated alkali metal compounds.

Compound	Scale / mmol	Yield / %	T_{dec} / °C
$Li_4[Ni(L1)_2]$ (**14-Li**) ·4 H_2O ·0.67 acetone	1.00	68	329
$Na_4[Ni(L1)_2]$ (**14-Na**)	1.00	74	345
$K_4[Ni(L1)_2]$ (**14-K**) ···H_2O	1.00	99	309
$K[Ni(HL1)(H_2L1)]$ (**14′-K**)	1.00	33	226
$Na_4[Pd(L1)_2]$ (**15-Na**)	0.50	73	362
$Na_4[Pt(L1)_2]$ (**16-Na**)	0.25	70	388
$Na_4[Cu(L1)_2]$ (**17-Na**)	1.00	73	279
$K_2[Cu(HL1)_2]$ (**17′-K**)	1.00	39	213
$Na_2[Ni(L2)_2]$ (**18-Na**) ·8 H_2O	1.00	47	298
$Na_2[Ni(L3)_2]$ (**21-Na**) ·4.5 H_2O	1.00	92	290

Table 2. Selected IR band positions $\tilde{\nu}$ (in cm^{-1}) for the isolated solids (in solvated form for **14-Li**, **14-K**, **18-Na**, and **21-Na**) and NMR shifts δ (in ppm) for carboxylic-acid functionalized transition metal complexes and their alkali metal salts. Unless otherwise noted, NMR spectra of the alkali metal compounds were measured in D_2O, and those of the parent carboxylic acids in DMSO-D_6.

Compound	ν(COO)	ν(M–S)	δ_C(COO)	δ_C(CSS)
$[Ni(H_2L1)_2]$ (**4**)[28]	1720, 1686	399, 392	168.0	208.9
$Li_4[Ni(L1)_2]$ (**14-Li**)	1686, 1600, 1507	394	173.5	207.1
$Na_4[Ni(L1)_2]$ (**14-Na**)	1590, 1498	394	173.6	207.1
$K_4[Ni(L1)_2]$ (**14-K**)	1594, 1504	387	173.5	207.0
$K[Ni(HL1)(H_2L1)]$ (**14′-K**)	1725, 1703, 1682, 1632, 1584, 1490	391	_ [a]	_ [a]
$[Pd(H_2L1)_2]$ (**5**)[28]	1706	363	168.5	213.4
$Na_4[Pd(L1)_2]$ (**15-Na**)	1590, 1493	?	173.7	210.9
$[Pt(H_2L1)_2]$ (**6**)[24]	1701, 1682	350	168.0	214.4
$Na_4[Pt(L1)_2]$ (**16-Na**)	1589, 1503	?	173.4	211.6
$[Cu(H_2L1)_2]$ (**7**)[25]	1723, 1684, 1641	336	–	–
$Na_4[Cu(L1)_2]$ (**17-Na**)	1590, 1485	357 ?	–	–
$K_2[Cu(HL1)_2]$ (**17′-Na**)	1700, 1601, 1504, 1485	348	–	–
$[Ni(HL2)_2]$ (**8**)	1703	385	170.8	202.1
$Na_2[Ni(L2)_2]$ (**18-Na**)	1631, 1582, 1500	383	177.1	200.3
$[Ni(HL3)_2]$ (**11**)	1726	394	167.5	208.1
$Na_2[Ni(L3)_2]$ (**21-Na**)	1634, 1597, 1509	392	172.9 [b]	209.9 [b]

[a] solubility insufficient for ^{13}C NMR spectroscopy, [b] in MeOH-D_4

remains virtually constant only for the Ni complexes, whereas a significant upfield shift is seen for Pd and Pt. In addition, the ^{195}Pt NMR signal of the $[Pt(L1)_2]^{4-}$ complex shifts slightly to lower field in going from **6** (−3919 ppm in DMSO-D_6)[24] to **16-Na** (−3843 ppm in D_2O). In order to verify if direct $COO^-\cdots M$ interactions in solution are relevant for the relatively oxophilic first-row transition metals Ni and Cu, we also recorded UV/Vis spectra for aqueous solutions of **4**/**14-Na** and **7**/**17-Na** (see Figures S7 and S8). In both cases, the positions of the absorption bands in the visible and near UV regions remain virtually unchanged upon metalation, so that significant direct $COO^-\cdots M$ interactions in solution can be ruled out. Regarding the comparison of the derivatives of different transition metals, both the IR and the NMR spectra of **14-Na**, **15-Na**, and **16-Na** are very similar, so that a close structural similarity within the series of the different group-10 metal complexes can be assumed. The ^1H and ^{13}C NMR spectra of **14-Li** and **14-K** are also virtually identical with those of **14-Na**, suggesting the existence of solvent-separated $[Ni(L1)_2]^{4-}$ ions and hydrated alkali metal cations in D_2O solution. This assumption agrees with the ^7Li and ^{23}Na NMR spectra, showing a sharp signal with a chemical shift close to 0 ppm. A similar picture was observed for the NMR spectra of **18-Na** and **21-Na**, each comprising one set of ligand ^1H and ^{13}C NMR signals and a sharp ^{23}Na NMR signal close to 0 ppm. The IR spectra of **14′-K** and **17′-K** are relatively rich of bands in the ν(COO) region and considerably different from each other, which confirms the partial deprotonation on the one hand and the different degree of metalation on the other hand (see Figure S5). The products were also characterized by ESI mass spectrometry, showing characteristic ion pairs of the complex anions with the respective alkali counterions. For the sodium salts of all complexes $[M(L1)_2]^{4-}$ (**14-Na–17-Na**), the most prominent peaks can be assigned to $[Na_5M(L1)_2]^+$, $[Na_4M(L1)(HL1)]^+$, $[Na_3M(L1)_2]^-$, and $[Na_2M(L1)_2]^{2-}$. In the case of the complexes comprising the monofunctional ligands L2 and L3, characteristic adducts are $[Na_2Ni(L)(HL)]^+$, $[NaNi(HL)_2]^+$, $[NaNi(L)_2]^-$, and $[Ni(L)(HL)]^-$. The finding that partially protonated species seem to be more stable than metal-rich species seems plausible in view of the smaller number of carboxylate ligators that are able to bind Na^+ ions efficiently. In addition, decarboxylation seems to occur more readily for L2 and L3 than for L1, as an intense peak of $[Ni(L)(HL)–CO_2]^-$ was detected for both **18-Na** and **21-Na**. The mass spectra of $A_4[Ni(L1)_2]$ (**14-Li/K**) are significantly different than those of their sodium congener, and no defined positively charged adducts could be assigned. Regarding negatively charged species, $[Li_3Ni(L1)_2]^-$ and $[Li_2M(L1)_2]^{2-}$ were observed for **14-Li** in analogy to **14-Na**, which does not apply to **14-K**. In this case, the ESI(−) mass spectrum is dominated by partially protonated species of low alkali metal content, namely $[K_2Ni(L1)(HL1)]^-$, $[KNi(HL1)_2]^-$, $[KNi(L1)(HL1)]^{2-}$, and $[Ni(HL1)_2]^{2-}$, which agrees with the picture of the softer K^+ ions that are more loosely bonded to carboxylate. A similar picture was observed for **14′** and **17′**.

Thermal decomposition. The solvated products are cleanly desolvated below 200 °C, followed by degradation of the $[M(L)_2]$ scaffold between ca. 200 and 400 °C (see Tables 1, S1 and S2, and Figures S9 and S10). As seen previously,[25,28] the thermal stabilities are substantially determined by the transition metal in the $M(DTC)_2$ core, following the order Cu < Ni < Pd < Pt for the T_{Dec} values. The thermal stabilities of the $Na_4[M(L1)_2]$-type compounds (**14-Na–16-Na**) are comparable with those of the related zinc derivatives $Zn_2[M(L1)_2]$ (M=Ni–Pt)[24,28] and considerably lower than for the alkaline-earth derivatives $AE_2[M(L1)_2]$ (M=Ni–Pt; AE=Mg–Ba).[25,29] By contrast, **17-Na** (T_{Dec} = 279 °C) is thermally considerably more stable than $Sr_2[Cu(L1)_2]$ which decomposes at 229 °C.[25] This difference might arise from the different coordination environment of the copper atom in both compounds (*vide infra*). The T_{Dec} values of the partially protonated derivatives **14′-K** and **17′-K** deviate fewer and are much lower than for the fully metallated congeners **14-Na** and

17-Na; apparently the presence of free carboxylic-acid moieties exerts a stronger influence on the thermal stability than the nature of the central $M(DTC)_2$ unit. A similar behavior has been observed previously with partially and fully deprotonated zinc derivatives of **6**.[24] Within the series $A_4[Ni(L1)_2]$ (**14**; A=Li–K), compound **14-Na** represents the thermally most stable entry, which fits with the lowest solubility of the sodium derivative and might represent another evidence for an efficient stabilization of the $[Ni(L1)_2]^{4-}$ ions by Na^+ counterions. Finally, comparison of **14-Na** with **18-Na** and **21-Na** reveals that the number of COONa functionalities in the molecule exerts a stronger influence on the thermal stability than the nature of the hydrocarbon backbone of the amino acid; the T_{Dec} values of **18-Na** and **21-Na** are similar and notably smaller than for **14-Na**. Similar observations have been made for $Zn_2[Pt(L1)_2]$ and $Zn[Pt(L2)_2]$, which were discussed with the different dimensionality of the coordination-polymeric assemblies resulting from carboxylate-metal linkages.[24]

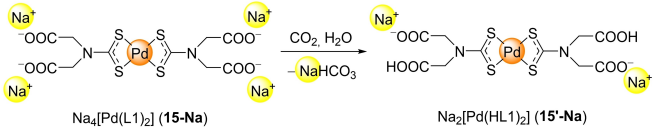

$Na_4[Pd(L1)_2]$ (**15-Na**) $Na_2[Pd(HL1)_2]$ (**15'-Na**)

Scheme 4. Probable transformation from **15-Na** to **15′-Na** through absorption of atmospheric CO_2.

Crystallization. In an extensive crystallization screening of a large number of alkali metal/transition metal/amino acid combinations, we were able to identify several well-crystalline phases of heterobimetallic alkali metal/transition metal compounds which were accessible to single-crystal structure analysis. While all attempts to prepare single crystals of the alkali-metal rich group-10 compounds $A_4[M(L1)_2]$ (M=Ni–Pt; **14–16**) failed, needle-like single crystals could be obtained for $Na_4[Cu(L1)_2]$ (**17-Na**)·9 H_2O and $Li_4[Cu(L1)_2]$ (**17-Li**)·*n* H_2O. By contrast, an attempt to crystallize $Na_4[Pd(L1)_2]$ (**15-Na**) afforded a small amount of single crystals of the partially protonated derivative $Na_2[Pd(HL1)_2]$ (**15′-Na**) in the form of an octahydrate, probably attributable to gradual acidification of the aqueous solution by absorption of atmospheric CO_2 upon standing (Scheme 4). These crystals could be reproduced by treatment of **5** with an understoichiometric amount of NaOH, but attempted isolation for the sake of full analytical characterization led to inseparable mixtures with **5**. More straightforward was the crystallization of the derivatives $Na_2[Ni(L2)_2]$ (**18-Na**) and $Na_2[Ni(L3)_2]$ (**21-Na**) in hydrated form. In addition, it could be shown that several other $A_2[M(L2)_2]$-type compounds (A/M=Na/Pd, K/Ni, K/Pd, K/Pt) as well as $Na_2[Pd(L3)_2]$ (**22-Na**) crystallize isotypically to the respective Na/Ni congeners, even though the crystal quality was not sufficient for full structure refinement. Important geometric parameters of the structurally characterized complexes and related compounds are summarized in Table 3.

In all structures, the thiophilic transition metal retains its all-sulfur coordination without any conspicuously close contacts to

Table 3. Selected geometric parameters of the metal atoms in the crystal structures of the reported alkali metal compounds and related compounds (ida = iminodiacetate; edta = ethylenediamine-*N*,*N*,*N*′,*N*′-tetraacetate). The parameter τ defines the twisting angle between the two CSS groups within the $M(DTC)_2$ fragment.

Compound	τ / deg.	M–S / pm	coord. no. A	A-OOC
Na(Hida) ···H_2O[38]	–	–	five	234.2(1)–259.6(1)
			six	234.6(1)–252.2(1)
Na_2(H_2edta) ·2 H_2O[39]	–	–	six	237.4(8)–256.9(8)
Na_4(edta) ·5 H_2O[39]	–	–	five	228.6(5)–234.4(5)
			six	229.2(5)–292.7(5)
			seven	230.3(6)–249.4(7)
$Na_2[Pd(HL1)_2]$ (**15′-Na**) ·8 H_2O	0.00	232.24(5)–232.64(4)	six	233.4(2)–235.2(1)
$Zn[Pd(HL1)_2]$ ·6 H_2O[28]	0.00	231.6(1)–232.4(1)	–	–
$[Cu(H_2L1)_2]$ (**7**) ·2 THF[25]	8.11(4)	227.7(1)–231.0(1)	–	–
$Na_4[Cu(L1)_2]$ (**17-Na**) ·9 H_2O	19.97(3)	230.86(8)–233.30(9)[a]	five	225.1(2)–234.2(2)
			six	226.8(2)–288.8(2)
K_2(H_2edta) ·2 H_2O[40]	–	–	seven	267.5(1)–312.7(1)
$K_2[Cu(HL1)_2]$ (**17′-K**)	0.00	229.53(9)–230.60(9)	eight	274.3(2)–305.4(2)
$Sr_2[Cu(L1)_2]$ ·9.5 H_2O[25]	0.00	231.1(1)–232.2(2)	–	–
$Na_2[Ni(L2)_2]$ (**18-Na**) ·*n* H_2O	10.83(8)	219.7(1)–221.4(1)	five ?	[b]
$Na_2[Ni(L3)_2]$ (**21-Na**) ·4.5 H_2O	2.29(2)–2.51(2)	219.61(5)–222.54(7)	five	229.4(2)–235.5(1)
			six	233.7(2)–238.1(2)
$Zn_2[Ni(L1)_2]$ ·14 H_2O[28]	0.00	219.12(5)–220.79(5)	–	–
$Zn_2[Ni(L1)_2]$ ·2.5 acetone ·8.5 H_2O[28]	0.00	219.3(2)–220.3(2)	–	–

[a] first coordination sphere formed by two κ^2S,S'-chelating groups. [b] Na–O bond lengths not reliable due to disorder.

oxygen donors, while the alkali metal ions are coordinated predominantly by oxygen (carboxylate, water). Less surprising, the hydrated group-10 derivatives **15′-Na**, **18-Na**, **18-K**, **19-Na**, **19-K**, **20-K**, **21-Na**, and **22-Na** all contain isolated, monomeric $M(DTC)_2$ units with a tetra-coordinate Ni, Pd, or Pt center.

Crystal structure of $Na_2[Pd(HL1)_2]$ (15′)·8 H_2O: The structure of **15′** ·8 H_2O (space group $P\bar{1}$) comprises two symmetry-independent Na sites, and all three metal atoms (Na1, Na2, Pd1) are situated on crystallographic centers of inversion (see Figure S13). The Pd–S bond lengths are in a very narrow range of 232.24(5)–232.64(4) pm and similar to those observed previously for $Zn[Pd(HL1)_2]\cdot 6\ H_2O$ (CSD: PALKAS), demonstrating that the oxophilic metal component in the heterobimetallic compounds can be varied without significant change of the $Pd(DTC)_2$ core. The residual acidic proton could be localized unambiguously, as the C–O bond lengths in the corresponding COOH group differ significantly (130.7(2) and 121.2(3) pm), whereas the same in the deprotonated COO group are very similar due to delocalization of the negative charge (126.1(2) and 125.1(2) pm). Somewhat surprising, only the protonated oxygen-donor group is coordinated to sodium, while the deprotonated one is fixed exclusively by O···H–O hydrogen bonds with water molecules. The COOH group links the two symmetry-independent Na atoms by κ*O*:κ*O*-bridging coordination of the carbonyl oxygen atom. A quite regular octahedral coordination is completed for both Na sites by four H_2O donors each (see Table S4). A similar octahedral *trans*-bis(carboxylate) arrangement has been seen previously with heterobimetallic DTCCs containing Co^{2+} or Ni^{2+} as the oxophilic metal.[29] The H_2O donors in **15′-Na** ·8 H_2O are coordinated in a μ-bridging mode, thus edge-linking the Na coordination octahedra into infinite chains in crystallographic *a*-axis direction. These chains are crosslinked by the $Pd(DTC)_2$ units, resulting in a 2D corrugated layer structure which is oriented parallel to the lattice plane (0 1 1) (Figure 1). As expected and previously seen with e.g. $Sr_2[Pd(L1)_2]$ ·4 H_2O (CSD: TOCFUQ), the $Pd(DTC)_2$ centers are well-separated and do not show any unusually close contacts between each other. The Na-coordination chains are additionally supported by O–H···O hydrogen bonds between alternating carboxylic acid and carboxylate groups. The hydrogen bond donors of the Na-coordinate H_2O molecules are oriented perpendicular to the layers and interconnect the layers together with non-coordinate H_2O molecules by a close net of hydrogen bonds.

Crystal structures of $Na_4[Cu(L1)_2]$ (17-Na)·9 H_2O and $Li_4[Cu(L1)_2]$ (17-Li)·*n* H_2O: In contrast to the complexes of the nickel group, the $Cu(DTC)_2$ units in **17-Na**·9 H_2O (space group C2/c) are part of a centrosymmetric, dimeric motif with penta-coordinate Cu atoms (Figure 2, see also Figure S14). The coordination is best described as a square-pyramidal [4 + 1] coordination, comprising four short (230.86(8)–233.30(9) pm) and one long Cu–S bond (277.37(8) pm), which defines the apical position and connects the two $Cu(DTC)_2$ parts. The significance of the fifth coordinative bond at copper reflects in the other four Cu–S bonds, which are significantly elongated as compared to the parent $[Cu(H_2L)_2]$ (**7**) containing tetra-coordinate copper (Cu–S 227.7(1)–231.0(1) pm).[25] Similar dimeric

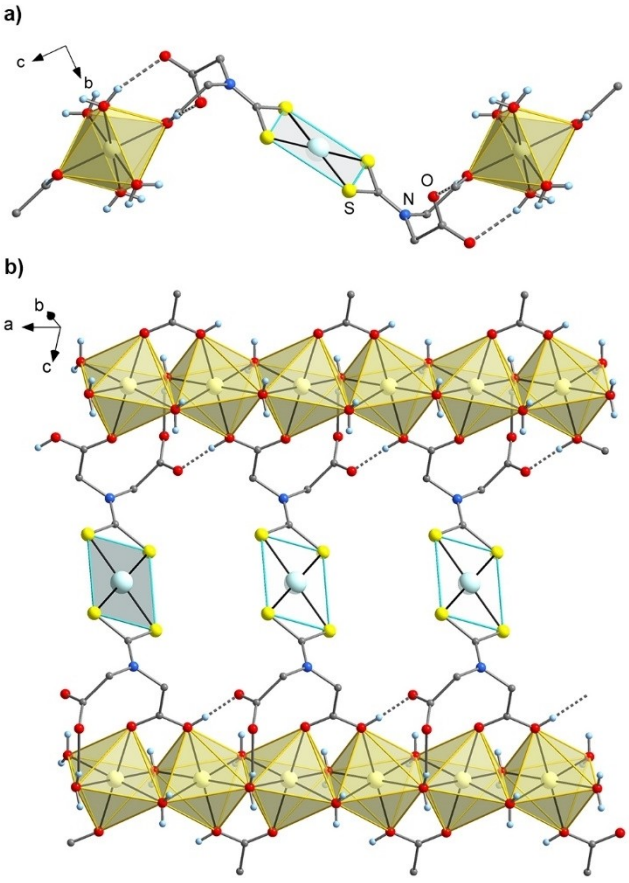

Figure 1. Extract of the polymeric layer structure in the crystals of $Na_2[Pd(HL1)_2]$ (**15′**)·8 H_2O, viewed in a projection on a) (1 0 0), and b) (0 1 1). Coordination polyhedra are highlighted for palladium (light turquoise) and sodium (yellow); all metal atoms are located on crystallographic centers of inversion.

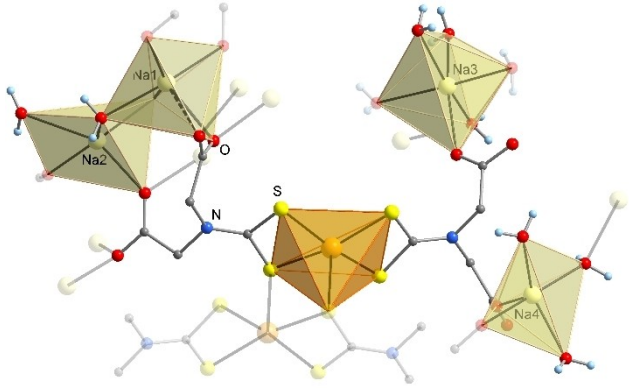

Figure 2. Extract of the crystal structure of $Na_4[Cu(L1)_2]$ (**17-Na**)·9 H_2O with highlighted coordination polyhedra of copper (orange) and sodium (yellow). Additional symmetry-equivalent $[Cu(L1)_2]^{4-}$ ions and Na atoms directly bound to the $[Cu(L1)_2]^{4-}$ ion are drawn semi-transparent. The resulting dimeric $[\{Cu(L1)_2\}_2]^{8-}$ unit exhibits crystallographically imposed inversion symmetry.

structures as for **17-Na**·9 H_2O have been reported for several other copper(II) bis(dithiocarbamate)s, e.g. $Cu(SSC\text{-}NEt_2)_2$ (CSD ref. code CETCAM01; Cu–S(equatorial) 229.9(1)–232.7(1) pm, Cu–S(apical) 284.4(1) pm) and $Cu(SSC\text{-}N^nPr_2)_2$ (CSD ref. code PRSCCU01; Cu–S(equatorial) 231.6(1)–232.2(1) pm, Cu–S(apical) 274.0(1) pm). Among the four symmetry-independent carboxylate groups in **17-Na**·9 H_2O, the two groups attached to the "exposed" κ^2S,S'-chelating DTC unit (S3, S4) are coordinated in a κO-monodentate mode to sodium. In contrast, the two COO^- groups at the $\kappa^2S,S':\kappa S$-bridging DTC unit (S1, S2) display highly bridging coordination modes, linking a total number of seven Na atoms. One of these donor groups (O3, O4) shows a rather symmetric $\kappa O:\kappa O:\kappa O':\kappa O'$ tetra-bridging σ-coordination, and the other (O1, O2) realizes a more asymmetric $\kappa^2O,O':\kappa O:\kappa O:\kappa O'$ mode. In the latter case, one of the bonds to the chelated Na atom (Na1) is considerably elongated to 288.8(2) pm, while the other Na–O(carboxylate) linkages at the same Na atom are in a range of 226.8(2)–242.6(2) pm. Geometrical analysis revealed that the coordination of this Na atom is best described as a [5 + 1] coordination in the shape of a capped trigonal bipyramid (see Table S4). In contrast to Na1, atom Na3 binds to only one carboxylate donor at an interatomic distance of 244.0(2) pm and is certainly coordinated in a distorted octahedral fashion. The two remaining Na atoms Na2 and Na4 are penta-coordinate with a median of Na–O(carboxylate) bonds considerably smaller than for Na3, ranging from 225.1(2) to 234.2(2) pm. While the coordination of Na2 is rather irregular, the coordination of Na4 fits well with a trigonal bipyramid.

An example of a structurally characterized sodium carboxylate with a similar number of sodium carboxylate groups in the molecule is Na_4(edta) ·5 H_2O (CSD: HACVEM), which also contains Na atoms with different coordination numbers at Na–O bond lengths comparable to as in **17-Na**·9 H_2O. Among the nine H_2O molecules in the asymmetric unit, three are coordinated in a μ-bridging and five in a terminal coordination with sodium, and one is non-coordinated. Due to the close net of Na-carboxylate linkages, the dimeric $[Cu(DTC)_2]_2$ motifs are interconnected to a dense three-dimensional structure. Despite this closely packed structure, the crystals of **17-Na**·9 H_2O decompose rapidly due to solvent loss upon isolation. Nonetheless, X-ray powder diffraction of the isolated **17-Na** revealed a high degree of crystallinity as well, similarly as observed for **14-Na**, **15-Na**, and **16-Na** (see Figure S19).

Even though the single-crystal diffraction data for the related **17-Li**·*n* H_2O did not allow for sufficient structure refinement, the interatomic connectivity referring to the $[Cu(L1)_2]^{4-}$ anions could be determined reliably and due to the high significance of this structure for this study, we decided to report the results herein (see Figure S15). Different from **17-Na**·9 H_2O, the $Cu(DTC)_2$ unit possesses crystallographically imposed inversion symmetry and is therefore strictly planar. These groups are stacked to an infinite linear assembly by close additional Cu···S contacts below 300 pm, so that the environment of the Cu centers can be described as a square-bipyramidal [4 + 2] coordination. A similar situation has been observed previously for $Sr_2[Cu(L1)_2]$·4 H_2O (CSD: TOCFUQ). The $[Cu(L1)_2]^{4-}$ anions are linked in a second dimension by centrosymmetric Li_2O_2 rings which are built through μ-bridging coordination of a carboxylate O atom of two adjacent $[Cu(L1)_2]^{4-}$ molecules. For these Li atoms, a distorted tetrahedral coordination is completed by another terminally κO-coordinated carboxylate and a H_2O ligand. A similar structural motif has been observed in the monohydrate of lithium dihydrogen citrate (CSD: PIGPUQ). Comparable cyclic $[Li_2O_2(L)_4]$ units (L = neutral O or N ligands) have been observed in numerous other lithium compounds with oxygen anions, e.g. with sterically demanding phenoxides,[34] alkoxides,[35] and siloxides.[36] The second Li atom in the asymmetric unit of hydrated **17-Li** is most likely part of disordered $[\{Li(H_2O)_n\}^+]_\infty$ chains that interpenetrate the anionic, three-dimensional network structure formed by the ···Cu(DTC)$_2$···Cu(DTC)$_2$··· and the ···Cu(DTC)$_2$···Li_2O_2··· linkages.

Crystal structure of $K_2[Cu(HL1)_2]$ (17′-K): The structure of anhydrous **17′-K** (space group $P\bar{1}$) contains centrosymmetric, thus strictly planar $Cu(DTC)_2$ units (Figure 3, see also Figure S16). Even though these building blocks are again stacked to linear infinite assemblies as seen with hydrated **17-Li**, the intermolecular Cu···S distances are beyond the sum of van-der-Waals radii and the coordination of the copper center should therefore be described as square-planar.[37] Consequently, the coordination environment of the transition metal in **17′-K** is more similar to that in the hydrate of the Pd complex **15′-Na** than in the related Cu complexes **17-Li** and **17-Na**. This situation also reflects in the Cu–S bond lengths, which are almost identical at 229.53(9) and 230.60(9) pm, thus being in a similar order of magnitude, but covering a much smaller range than in the parent $[Cu(H_2L)_2]$ (**7**) which contains a significantly twisted $Cu(DTC)_2$ core.[25] Similar structures with inversion-symmetric, non-aggregated $Cu(DTC)_2$ units have been reported for numerous other copper bis(dithiocarbamate)s, e.g. the di-isopropyl (CSD: NDTCCU02; Cu–S 228.5(1)–29.229.1(1) pm), the di-*n*-butyl (CSD: UKEDAP; Cu–S 226.8(1)–230.2(1) pm), and the ethyl *n*-butyl (CSD: UKEDOD; Cu–S 229.2(1)–230.1(1) pm) derivatives. The potassium atom displays an irregular eight-coordination (see Table S4), which is not only completed by carboxylate oxygen donors, but also by a direct K–S contact (337.4(1) pm). Among the seven oxygen donors, four are part of chelating

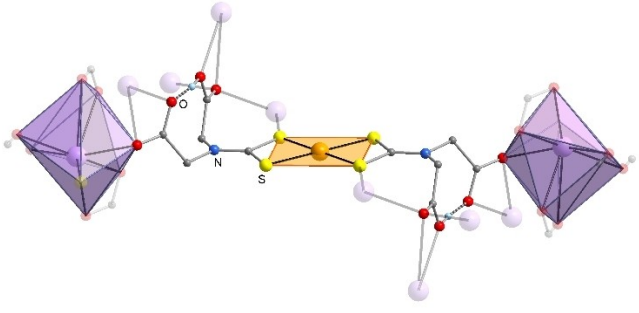

Figure 3. Extract of the crystal structure of $K_2[Cu(HL1)_2]$ (**17′-K**) with highlighted coordination polyhedra of copper (orange) and potassium (violet). Additional symmetry-equivalent K atoms directly bound to the $[Cu(HL1)_2]^{2-}$ ion are drawn semi-transparent. The Cu atom is situated on a crystallographic center of inversion.

COO moieties, whereas the other three are singly coordinated oxygen donors. The residual acidic proton seems to be localized at one of the two COO groups of the L1 ligand, where the corresponding C–O bond lengths are in good agreement with a distinct single or double bond, respectively (C3–O3 130.3(3) pm and C3–O4 121.2(3) pm). The difference in C–O distances in the other (deprotonated) COO group is smaller, but still significant (C1–O1 122.6(3) pm, C1–O2 127.4(4) pm). This is most likely due to sharing of the acidic proton between the two COO groups in terms of an intramolecular O–H···O hydrogen bond, interfering with charge delocalization within the COO^- group. The assumedly protonated COO group is attached to a total of four K atoms (coord. mode $\kappa^2O,O':\kappa O:\kappa O$), while there are only two K atoms bound to the deprotonated COO group (coord. mode $\kappa^2O,O':\kappa O$). As a result of this connectivity pattern, a dense three-dimensional network is formed.

Crystal structures of $Na_2[Ni(L2)_2]$ (18-Na) ·*n* H_2O and related compounds: The hydrates of **18-Na** and its heavier homologs **18-K**, **19-Na/K**, and **20-K** crystallize in the highly symmetric space group I222, with the transition metal atom residing on a 2-axis (see Figure S17). Due to the crystallographically imposed rotational symmetry, the two carboxylate groups are in an *anti*-arrangement. The coordination plane of the Ni atom in hydrated **18-Na** is unusually strongly twisted along the C6–C6′ vector (angle between NiS_2 planes: 10.83(8)°). This effect is rather typical for Cu(II) analog complexes,[25] whereas there are only few examples for structurally characterized Ni(II) bis(dithiocarbamate)s where the absence of crystallographically imposed inversion symmetry on the metal center enables deviation from planarity. The twisting of the two DTC ligands is usually much slighter than found in **18-Na**; examples of derivatives with relatively large angles between the NiS_2 planes are those where the $Ni(DTC)_2$ fragment is part of a macrocyclic system (ELUFOG, 3.45(3)°, and IXIVUG, 5.7(2)°), as well as $Ni(SSC–N(Bn)CH_2-C_6H_4-4-OH)_2$ (FORNEI, 1.37(4)–4.98(3)°). While the $[Ni(L2)_2]^{2-}$ complex is well-ordered in the crystal structure of hydrated **18-Na**, the Na^+ counterions are massively disordered. The structure contains assumedly one equiv. of $[Na(H_2O)_5]^+$ cations, which is linked with the carboxylate groups through O–H···O hydrogen bonds and site-disordered in crystallographic *a*-axis direction. The missing equiv. Na^+ per formula unit is probably (in the form of $[Na(H_2O)_n]^+$ as well) fully disordered and situated within large channels in *a*-axis direction (Figure 4). Since half of the hydrated sodium cations could not be refined, we also examined the possibility of crystallization of a sodium-deficient species as it has been observed with **15′-Na**. The carboxylate C–O bond lengths are virtually identical at 126.3(8) and 126.8(8) pm, suggesting full deprotonation. In addition, crystallization under an inert atmosphere (exclusion of acidic atmospheric CO_2) led to an identical result, so that the formation of a partially protonated species seems highly improbable. The low degree of ordering of the Na^+ ions in hydrated **18-Na** makes it plausible why isotypic structures are formed with K^+ ions, as seen with **18-K**, **19-K**, and **20-K**. Even though these structures could not be fully refined, the conformation of the $[M(L2)_2]^{2-}$ anion could be determined with sufficient precision, showing that the exchange of Na^+ by K^+ counterions results in an even stronger deformation of the $Ni(DTC)_2$ unit (angle between NiS_2 planes 11.2(3)° in **18-K**, Figure 5, a). Comparison of **18-K** with its heavier transition-metal homologs **19-K** and **20-K** revealed that the deviation from planarity decreases in going from Ni to Pd (9.1(2)°) to Pt (7.3(2)°), which meets the expectation in view of the increasing preference of a square-planar coordination in the same direction (Figure 5, b). However, the twisting angle of about 7° for the Pt complex is still remarkable and larger than in the related $Zn[Pt(L3)_2]\cdot 6\ H_2O$ (5.0(2)°; CSD: GUCQIH).

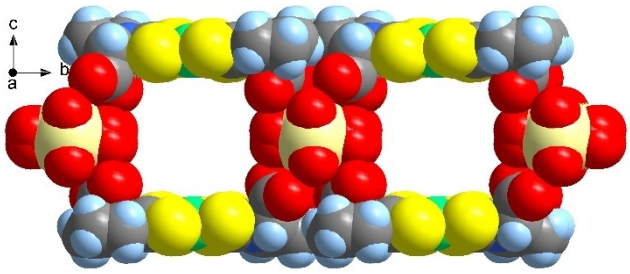

Figure 4. Representation of the supramolecular double-layer structure of **18-Na** ·*n* H_2O by a space-filling model, illustrating the existence of large channels in crystallographic *a*-axis direction (viewed in a projection on (1 0 0); color code: Ni = green, S = yellow, O = red, N = blue, C = grey, H = light blue). The double layer extends parallel to the lattice plane (0 0 1).

Crystal structure of $Na_2[Ni(L3)_2]$ (21-Na)·4.5 H_2O: Compound **21-Na** ·4.5 H_2O exhibits a relatively complex crystal structure, comprising two formula units in the asymmetric unit (space group $P2_1/c$; Figure S18). The Ni–S bonds are 219.61(5)–222.54(7) pm and therefore marginally longer than in hydrated **18-Na** and in $Zn_2[Ni(L1)_2]$ (CSD: PAKWEH, PAKWIL). Due to the missing crystallographic inversion symmetry on the two Ni sites, the $Ni(DTC)_2$ units are not strictly planar, but are twisted only marginally by about 2–3°. Another difference to the $[Ni(L2)_2]^{2-}$

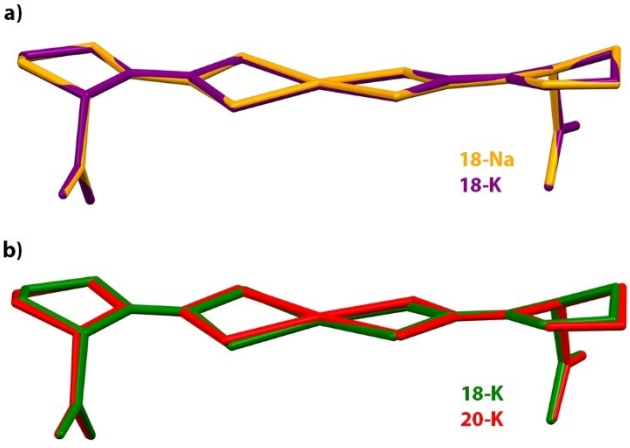

Figure 5. Molecule overlay of $[M(L2)_2]^{2-}$ ions in the crystal structures of different $A_2[M(L2)_2]$ derivatives (**18–20**), illustrating the influence of a) the alkali metal A, and b) the transition metal M on the conformation of the $M(DTC)_2$ core.

ion in hydrated **18-Na** is that the two asymmetric amino-acid residues in the $[Ni(L3)_2]^{2-}$ anion are *syn*-arranged and therefore similar as in the parent carboxylic acid **11**, suggesting that the amino-acid residue is not able to rotate freely around the dithiocarbamate C–N bond in solution. All four carboxylate groups in the asymmetric unit display different coordination modes, including $\kappa O:\kappa O':\kappa O'$ tetra-bridging, $\kappa O:\kappa O:\kappa O'$ tri-bridging, and κO-monodentate modes, as well as a non-coordinate COO^- group. The coordination of the four symmetry-independent Na atoms by carboxylate and water oxygen donors is also significantly different, including one hexa-coordinate, distorted octahedral site (Na2), and three penta-coordinate sites with different geometries (Na1, Na3, Na4; see Table S4). Na4 is coordinated exclusively by water donors, whereas the other three Na atoms display mixed coordination by carboxylate and water. Geometrical analysis revealed a rather unusual coordination in the shape of a vacant octahedron for Na1 and Na3. Both Na atoms are in spacial proximity to a $Ni(DTC)_2$ unit and the sixth coordination site might be occupied by some direct Na···S attraction. For Na1 (Na1–S1 360.5(1) pm) this interaction seems to be more significant than for Na3 (Na3–S5 404.0(1) pm), where the Na···S separation is in the range of the van-der-Waals sum.[37] The coordination of Na4 fits best with a distorted square-bipyramid, even though there is another close Na···S contact to an adjacent $Na(DTC)_2$ unit (Na4–S7 378.85(8) pm). In contrast to Na1 and Na3, this additional contact does not result in a defined coordination polyhedron, so that it can be assumed that the resulting coordination angles are more significant for the evaluation of attractive Na···S interactions than the interatomic distance alone. The nine equiv. H_2O in the asymmetric unit comprise five μ-bridging and three terminally coordinated H_2O ligands together with one non-coordinated water molecule of crystallization. The different building blocks are assembled into infinite two-dimensional sheets featuring a rather complicated pattern of edge- and corner-linked Na coordination polyhedra (Figure 6). Remarkedly, hydrogen bonds extend predominantly within the layer structure, whereas the layers are separated through the hydrophobic benzyl groups situated on the surface. X-ray powder diffraction showed that the isolated bulk product of **21-Na**·4.5 H_2O is also well crystalline (Figure S20). However, despite a similar water content, the diffractogram does not match the pattern calculated from the single-crystal data, which might be due to the formation of different polymorphs.

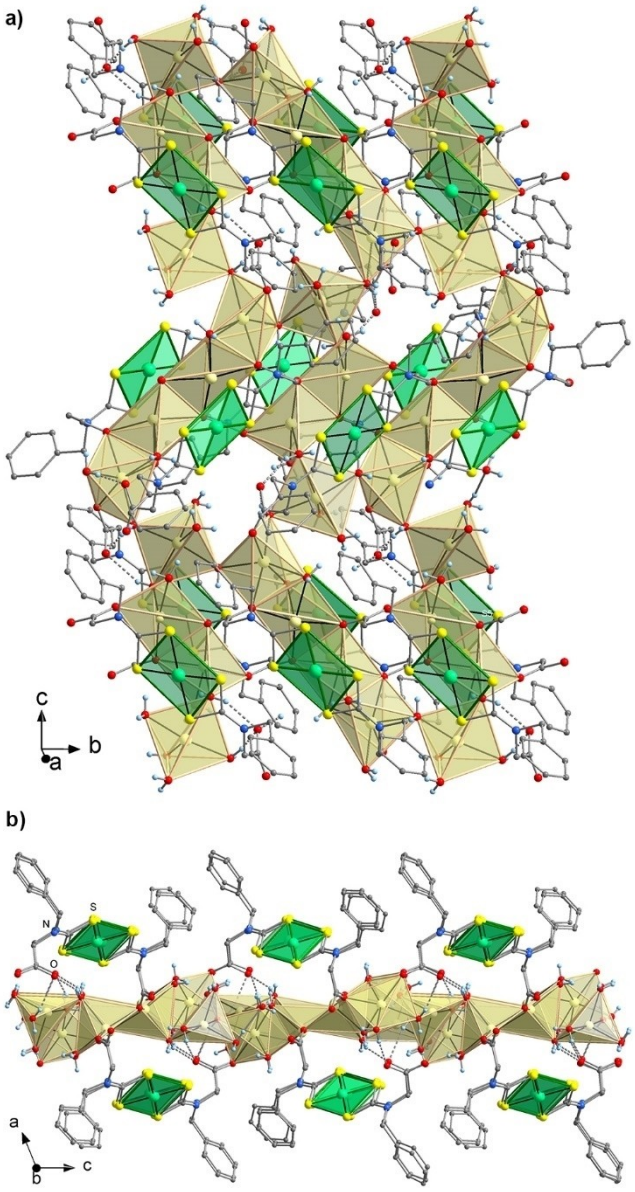

Figure 6. Extract of the polymeric layer structure in the crystals of $Na_2[Ni(L4)_2]$ (**21-Na**) ·4.5 H_2O, viewed in a projection on a) (0 0 1) and b) (0 1 0). Coordination polyhedra are highlighted for nickel (green) and sodium (yellow); all metal atoms are located on general crystallographic sites.

Conclusions

The preparation and extensive analytical characterization of alkali-carboxylate functionalized bis(DTC) complexes of bivalent nickel, palladium, platinum, and copper derived from different α-amino acids was performed. Comparison of the different transition metal derivatives as exemplified with the series $Na_4[M(L1)_2]$ resembled the findings observed previously with the derivatives of other oxophilic metals. The group-10 metals contribute very similarly to the molecular structures and properties of the products,[25,28] while the Cu compounds behave significantly differently and are structurally more diverse.[25] The alkali metals are structurally highly flexible, and in contrast to the strongtransition-metal DTC coordination, the alkali-metal carboxylate binding is of predominantly ionic nature and should be regarded as rather weak. It has been seen that there is competition between 1) coordination of the alkali metal atoms by carboxylate vs. solvent water, and 2) metal coordination vs. hydrogen bonding of the carboxylate groups; both effects lead to an unpredictable number of carboxylate donors and carboxylate/water ratio in the coordination sphere of the alkali metal atoms. In addition, steric saturation is more relevant

for the alkali and alkaline-earth metals than the realization of defined coordination polyhedra, so that the overall structures of the products are hardly predictable. Nonetheless, some typical trends can be seen in the series of the different group-1 metals, e.g. the increase of the average coordination number and the decrease of solvent coordination in going from Li to Na to K. It was shown that the choice of the alkali metal influences the stabilization of complex counterions with different degrees of protonation, as well as the physical properties of the products. For instance, the potassium salts are significantly soluble in organic media, which opens potential pathways to new reaction conditions. $K_2[Cu(HL1)_2]$ (**17′-K**) is a rare example of a hard/soft-heterobimetallic AA-DTC which shows direct bonding between the oxophilic metal and the sulfur donors in its crystal structure. The preparation and structural characterization of related compounds of the heaviest alkali metals Rb and Cs, in order to evaluate the impact of direct A···S interactions on the structure and reactivity of the $M(DTC)_2$ core, will be the objective of future research. Even though the spectroscopic and structural data collected in this study have shown that there is no significant direct interaction between the carboxylate functionalities and the transition metal center in the solid state and in solution, there might be an indirect structural impact by the close net of A-carboxylate linkages and O–H···O hydrogen bonds in the solid state. This might probably support the aggregation of $Cu(DTC)_2$ units to dimeric or polymeric assemblies as seen with $Li_4[Cu(L1)_2]$ (**17-Li**) and $Na_4[Cu(L1)_2]$ (**17-Na**), and force the transition metal into unusual coordination geometries, as observed for compounds of the series $A_2[M(L2)_2]$ (**18–20**) exhibiting markedly twisted DTC ligands. Ligands derived from chiral amino acids appear particularly useful in this context as they block the effect of structural confinement by crystallographically imposed inversion symmetry on the transition-metal center.

Experimental Section

General. Unless otherwise stated, all operations were performed under atmospheric conditions without exclusion of air. All starting materials and solvents were obtained from commercial suppliers and used without further purification. NMR spectra were recorded on a Bruker AVIII 400 or a Bruker Advance 400 MHz machine (5 mm BBO; ^{1}H: 400.1 MHz, ^{13}C: 100.6 MHz) at ambient temperature. Chemical shifts are referenced to external standards as follows (0 ppm each): tetramethylsilane (for ^{1}H and ^{13}C), 9.7 mol/L LiCl in D_2O (for ^{7}Li), 0.1 mol/L NaCl in D_2O (for ^{23}Na), and 1.2 mol/L $Na_2[PtCl_6]$ in D_2O (for ^{195}Pt). Unless otherwise noted, the given signals are singlets. IR spectra were measured on a Bruker Vertex 70 FTIR spectrometer equipped with a diamond ATR unit, and ESI mass spectra on a Thermo LTQ machine applying the ESI-positive and the ESI-negative mode. UV/Vis spectra were measured on a Varian Cary5000 spectrometer. Elemental analyses (EA) were performed using a HEKAtech Eurovector EA3000 CHNS analyzer. Thermal analyses (TG/DTA) were performed using a Netzsch STA 449F1 Jupiter thermobalance. The samples were measured in a temperature range from room temperature to 600 °C with a heating rate of 10 K/min under nitrogen. The X-ray crystallographic data are summarized in Table S3 in the Supplementary Information. The crystal structures were solved with SHELXT-2018/3[41] and refined by full matrix least-squares methods on F^2 with SHELXL-2018/3,[42] using the Olex2 1.5 environment.[43] For **18-Na**·*n* H_2O, diffuse electron density by disordered $[Na(H_2O)_n]^+$ and H_2O was taken into account by the solvent-mask routine of Olex2 1.5. The geometric environment of the alkali metal atoms was analysed on the basis of continuous symmetry measures using SHAPE 2.1.[44] X-ray powder diffractograms were measured in capillaries with 0.2–0.5 mm diameter at ambient temperature, on a Stoe Stadi P diffractometer, using Cu–Kα radiation. Deposition numbers 2353080–2353085 contain the supplementary crystallographic data for this paper. These data are provided free of charge by the Cambridge Crystallographic Data Center (http://www.ccdc.cam.ac.uk/).

Synthesis of bis(dithiocarbamato) complexes 4–13. All carboxylic-acid functionalized complexes were prepared by a standard procedure by allowing a suitable transition-metal salt to react with two equiv. of the respective ligand **1–3** (as Na or K salt)[45] in aqueous solution. The applied procedures have been reported recently for the preparation of the iminodiacetic-acid derived complexes **4** and **5**,[28] **6**,[24] and **7**,[25] and was now applied to the also known L-proline derivatives **8**,[13,14,18,20] **9**,[18] and **10**,[18,24] as well as to the new *N*-benzylglycine derivatives **11–13**. For a typical preparation of the latter, 1 equiv. of the specific metal precursor is added to an aqueous solution of 2 equiv. Na_2(L3) (**3-Na**) or K_2(L3) (**3-K**) as detailed below. After the complex formation is complete, 2 equiv. hydrochloric acid (1.0 mol/L) is added and stirring is continued for 1 h. The precipitated product is isolated by vacuum filtration over a P3 frit, washed thoroughly with water and dried in a desiccator over conc. H_2SO_4. The isolated products are soluble in DMSO, sparingly soluble in ethanol and acetone, and insoluble in chloroform and water.

$[Ni(HL3)_2]$ (**11**): $NiCl_2$ ·6 H_2O (7.5 mmol, 1.78 g) was allowed to react with **3-Na**·4 H_2O (15 mmol, 5.36 g)* in a total volume of 60 ml water. The solution turned dark green immediately, and the product was precipitated with hydrochloric acid after 15 min. Yield: 3.70 g (84 %). Yellowish-green powder, T_{Dec} = 230 °C. EA calcd. for $C_{20}H_{20}N_2NiO_4S_4$ (M = 539.32 g/mol): C 44.54, H 3.74, N 5.24, S 22.81 %; found: C 44.57, H 3.68, N 5.19, S 23.78 %. ^{1}H NMR (DMSO-D_6): δ 4.23 (2H; CH_2COOH), 4.83 (2H; CH_2Ph), 7.32–7.42 (m, 5H; *CH* Ph), 13.32 (br, 1H; COO*H*) ppm. ^{13}C NMR (DMSO-D_6): δ 49.7 (CH_2COOH), 53.1 (CH_2Ph), 128.1 (*p*-*C*H Ph), 128.2 (*o*-*C*H Ph), 128.7 (*m*-*C*H Ph), 134.0 (*i*-*C* Ph), 167.5 (*C*OOH), 208.1 (*C*SS) ppm. ESI(+)-MS: *m/z* 1100.3 (69 %; [2 M + Na]$^+$), 561.0 (100 %; [M + Na]$^+$). ESI(−)-MS: *m/z* 1076.1 (34 %; [2 M –H]$^-$), 536.8 (100 %; [M –H]$^-$), 492.9 (82 %; [M –H –CO_2]$^-$). *The use of in-situ prepared instead of isolated **3-Na** or **3-K** led to comparable results. Single crystals of **11** ·DMSO suitable for X-ray structural analysis were obtained from a solution in DMSO/methanol (1 : 3) at −25 °C.

$[Pd(HL3)_2]$ (**12**): $PdCl_2$ (4 mmol, 0.71 g) was allowed to react with **3-Na** ·4 H_2O (8 mmol, 2.86 g) in a total volume of 50 ml water. The resulting suspension was stirred at r.t. for 72 h before the product was precipitated with hydrochloric acid. Yield: 2.03 g (86 %). Ocher-yellow powder, T_{Dec} = 253 °C. EA calcd. for $C_{20}H_{20}N_2O_4PdS_4$ (M = 587.05 g/mol): C 40.92, H 3.43, N 4.77, S 21.84 %; found: C 40.25, H 3.23, N 5.01, S 20.99 %. ^{1}H NMR (DMSO-D_6): δ 4.37 (2H; CH_2COOH), 4.95 (2H; CH_2Ph), 7.31–7.41 (m, 5H; *CH* Ph), 13.29 (br, 1H; COO*H*) ppm. ^{13}C NMR (DMSO-D_6): δ 50.0 (CH_2COOH), 53.4 (CH_2Ph), 128.1 (*p*-*C*H Ph), 128.2 (*o*-*C*H Ph), 128.7 (*m*-*C*H Ph), 134.1 (*i*-*C* Ph), 167.7 (*C*OOH), 211.9 (*C*SS) ppm. ESI(+)-MS: *m/z* 1781.3 (43 %; [3 M + Na]$^+$), 1198.3 (100 %; [2 M + Na]$^+$), 609.1 (57 %; [M + Na]$^+$). ESI(−)-MS: *m/z* 1757.7 (21 %; [3 M−H]$^-$), 1172.2 (100 %; [2 M−H]$^-$), 586.7 (98 %; [M−H]$^-$).

$[Pt(HL3)_2]$ (**13**): K_2PtCl_4 (1.25 mmol, 0.519 mg) was allowed to react with **3-Na**·4 H_2O (2.5 mmol, 893 mg) in a total volume of 30 ml water. The resulting clear, orange solution was stirred at r.t. for 4 h

before the product was precipitated with hydrochloric acid. Yield: 730 mg (86 %). Yellow-orange powder, T_{Dec} 258 °C. EA calcd. for $C_{20}H_{20}N_2O_4PtS_4$ (M = 675.71 g/mol): C 35.55, H 2.98, N 4.15, S 18.98 %; found: C 35.88, H 2.93, N 4.02, S 18.77 %. ^{1}H NMR (DMSO-D_6): δ 4.23 (2H; CH_2COOH), 4.82 (2H; CH_2Ph), 7.32–7.42 (m, 5H; C*H* Ph), 12.95 (br, 1H; COO*H*) ppm. ^{13}C NMR (DMSO-D_6): δ 49.9 (*C*H_2COOH), 53.6 (*C*H_2Ph), 128.2 (*p*-*C*H Ph), 128.3 (*o*-*C*H Ph), 128.8 (*m*-*C*H Ph), 134.0 (*i*-*C* Ph), 167.7 (*C*OOH), 213.2 (*C*SS) ppm. ^{195}Pt NMR (DMSO-D_6): δ −3.900 ppm. ESI(+)-MS: *m/z* 1373.5 ([2 M + Na]$^+$), 698.1 (100 %; [M + Na]$^+$). ESI(−)-MS: *m/z* 1350.3 (38 %; [2 M–H]$^-$), 673.8 (100 %; [M–H]$^-$), 587.0 (82 %; [M–H–2 CO_2]$^-$).

Synthesis of alkali metal compounds 14–23. To a suspension of the parent carboxylic-acid derivative **4–13** in water, the respective alkali metal hydroxide as an aqueous solution was added. The mixture was stirred at ambient temperature until the starting material had completely dissolved, and the product was isolated as detailed below. Even though strict exclusion of air is not necessary, the contact to air was minimized during all working steps in order to avoid interfering reactions with atmospheric CO_2 (formation of A_2CO_3 or $AHCO_3$; A=Li, Na, or K),

$Li_4[Ni(L1)_2]$ (**14-Li**): Upon addition of LiOH solution (4.2 ml, 1.0 mol/L, 4.2 mmol), a suspension of $[Ni(H_2L1)_2]$ (**4**; 1.0 mmol, 475 mg) in water (20 ml) turned into a clear solution within few minutes. The solution was evaporated to dryness on a rotary evaporator at 40 °C, the solid residue washed with acetone and dried *in vacuo*. Yield: 416 mg (68 % based on **14-Li** ·4 H_2O ·0.67 acetone). Olive-green powder, very soluble in water and insoluble in acetone, T_{Dec} = 329 °C. EA calcd. for $C_{12}H_{20}Li_4N_2NiO_{12.67}S_4$ (M = 609.85 g/mol): C 23.65, H 3.31, N 4.59 %; found: C 23.52, H 3.58, N 4.92 %. ^{1}H NMR (D_2O): δ 1.28 (4H; CH_3 acetone), 4.19 (8H; CH_2) ppm. ^{13}C NMR (D_2O): δ 28.2 (*C*H_3 acetone), 53.5 (*C*H_2), 173.5 (*C*OO$^-$), 207.1 (*C*SS), 215.0 (*C*O acetone) ppm. ^{7}Li NMR (D_2O): δ 0.15 ppm. ESI(−)-MS: *m/z* 491.0 ([$Li_3Ni(L1)_2$]$^-$), 239.1 ([$Li_2Ni(L1)_2$]$^{2-}$).

$Na_4[Ni(L1)_2]$ (**14-Na**):[16] Upon addition of NaOH solution (4.2 ml, 1.0 mol/L, 4.2 mmol), a suspension of $[Ni(H_2L1)_2]$ (**4**; 1.0 mmol, 475 mg) in water (20 ml) turned into a clear solution within few minutes. Acetone (50 ml) was added under stirring, and the mixture was subsequently stored at 5 °C for several hours to maximize precipitation of the product. The solid was isolated by vacuum filtration over a P3 frit, dried in air overnight and then in a desiccator over conc. H_2SO_4. Yield: 416 mg (74 % based on anhydrous **14-Na**). Yellow-green powder, very soluble in water and insoluble in acetone, T_{Dec} = 345 °C. EA calcd. for $C_{10}H_8N_2Na_4NiO_8S_4$ (M = 563.07 g/mol): C 21.33, H 1.43, N 4.98 %; found: C 21.29, H 1.47, N 4.93 %. ^{1}H NMR (D_2O): δ 4.20 (8H; CH_2) ppm. ^{13}C NMR (D_2O): δ 53.5 (*C*H_2), 173.6 (*C*OO$^-$), 207.1 (*C*SS) ppm. ^{23}Na NMR (D_2O): δ 0.2 ppm. ESI(+)-MS: *m/z* 584.9 ([$Na_5Ni(L1)_2$]$^+$). ESI(−)-MS: *m/z* 538.8 ([$Na_3Ni(L1)_2$]$^-$), 494.8 ([$Na_3Ni(L1)_2$ –CO_2]$^-$), 258.0 ([$Na_2Ni(L1)_2$]$^{2-}$).

$K_4[Ni(L1)_2]$ (**14-K**): Compound **14-K** was prepared similarly as described for **14-Li**, using the given amount of KOH instead of LiOH solution. Yield: 639 mg (99 % based on **14-K** ·H_2O). Olive-green powder, very soluble in water and slightly soluble in acetone, T_{Dec} = 309 °C. EA calcd. for $C_{10}H_{10}K_4N_2NiO_9S_4$ (M = 645.52 g/mol): C 18.61, H 1.56, N 4.34 %; found: C 18.28, H 1.43, N 4.32 %. ^{1}H NMR (D_2O): δ 4.20 (8H; CH_2) ppm. ^{13}C NMR (D_2O): δ 53.5 (*C*H_2), 173.5 (*C*OO$^-$), 207.0 (*C*SS) ppm. ESI(−)-MS: *m/z* 548.7 ([$K_2Ni(L1)(HL1)$]$^-$), 510.9 ([$KNi(HL1)_2$]$^-$), 254.9 ([$KNi(L1)(HL1)$]$^{2-}$), 236.0 ([$Ni(HL1)_2$]$^{2-}$).

K[Ni(HL1)(H_2L1)] (**14′-K**): Upon addition of KOH solution (2.0 ml, 1.0 mol/L, 2.0 mmol) to a suspension of $[Ni(H_2L1)_2]$ (**4**; 1.0 mmol, 475 mg) in water (18 ml), a flocculent precipitate began to form after few seconds. Stirring at r.t. was continued overnight and the mixture subsequently stored at 5 °C to maximize precipitation of the product. The solid was isolated by vacuum filtration over a P4 frit, washed with a small amount of ice water, and dried in a desiccator over conc. H_2SO_4. Yield: 170 mg (33 % based on anhydrous **14′-K**). Yellow-green powder, sparingly soluble in water and insoluble in organic solvents, T_{Dec} = 226 °C. EA calcd. for $C_{10}H_{11}KN_2NiO_8S_4$ (M = 513.24 g/mol): C 23.40, H 2.16, N 5.46 %; found: C 23.39, H 2.45, N 5.87 %. ^{1}H NMR (D_2O): δ 4.25 (8H; CH_2) ppm, COO*H* not observed. ESI(−)-MS: *m/z* 510.9 ([$KNi(HL1)_2$]$^-$), 472.8 ([$Ni(HL1)(H_2L1)$]$^-$), 255.0 ([$KNi(L1)(HL1)$]$^{2-}$), 236.0 ([$Ni(HL1)_2$]$^{2-}$).

$Na_4[PdL1)_2]$ (**15-Na**): Compound **15-Na** was prepared similarly as described for **14-Na** by reaction of $[Pd(H_2L1)_2]$ (**5**; 0.5 mmol, 261 mg) with NaOH (2.1 ml, 1.0 mol/L, 2.1 mmol), in water (10 ml). Yield: 222 mg (73 % based on anhydrous **15-Na**). Pale yellow powder, very soluble in water and insoluble in acetone, T_{Dec} = 362 °C. EA calcd. for $C_{10}H_8N_2Na_4O_8PdS_4$ (M = 610.80 g/mol): C 19.66, H 1.32, N 4.59 %; found: C 19.51, H 1.22, N 4.36 %. ^{1}H NMR (D_2O): δ 4.32 (8H; CH_2) ppm. ^{13}C NMR (D_2O): δ 53.7 (*C*H_2), 173.7 (*C*OO$^-$), 210.9 (*C*SS) ppm. ^{23}Na NMR (D_2O): δ 0.2 ppm. ESI(+)-MS: *m/z* 633.0 ([$Na_5Pd(L1)_2$]$^+$), 610.9 ([$Na_4Pd(L1)(HL1)$]$^+$). ESI(−)-MS: *m/z* 588.8 ([$Na_3Pd(L1)_2$]$^-$), 442.8 ([$Na_3Pd(L1)_2$ –CO_2]$^-$), 283.0 ([$Na_2Pd(L1)_2$]$^{2-}$). Slow evaporation of aqueous solutions of **15-Na** at r.t. with the objective to grow single crystals led occasionally to the formation of few crystals of **15′-Na** ·8 H_2O.

$Na_2[Pd(HL1)_2]$ (**15′-Na**): To a suspension of $[Pd(H_2L1)_2]$ (**4**; 0.5 mmol, 261 mg) in water (10 ml), a minimum amount of NaOH solution required for complete dissolution of the complex within one hour was added (approx. 0.5 ml, 1.0 mol/L, 0.5 mmol). The orange solution was allowed to evaporate slowly at r.t., resulting in the formation of orange, prism-like single crystals of **15′-Na** ·8 H_2O suitable for X-ray structural analysis within few days. Attempts to isolate the product for full analytical characterization led to inseparable mixtures with **4**.

$Na_4[PtL1)_2]$ (**16-Na**): Compound **16-Na** was prepared similarly as described for **14-Na** by reaction of $[Pt(H_2L1)_2]$ (**6**; 0.25 mmol, 153 mg) with NaOH (1.05 ml, 1.0 mol/L, 1.05 mmol), in water (10 ml). Yield: 123 mg (70 % based on anhydrous **16-Na**). Pale yellow powder, very soluble in water and insoluble in acetone, T_{Dec} = 388 °C. EA calcd. for $C_{10}H_8N_2Na_4O_8PtS_4$ (M = 699.46 g/mol): C 17.17, H 1.15, N 4.01 %; found: C 17.04, H 1.03, N 3.84 %. ^{1}H NMR (D_2O): δ 4.18 (8H; CH_2) ppm. ^{13}C NMR (D_2O): δ 53.6 (*C*H_2), 173.4 (*C*OO$^-$), 211.6 (*C*SS) ppm. ^{195}Pt NMR (D_2O): δ −3.843 ppm. ^{23}Na NMR (D_2O): δ 0.2 ppm. ESI(+)-MS: *m/z* 720.9 ([$Na_5Pt(L1)_2$]$^+$), 701.0 ([$Na_4Pt(L1)(HL1)$]$^+$). ESI(−)-MS: *m/z* 909.5 ([$Na_4Pt(L1)(HL1)_2$]$^-$), 675.1 ([$Na_3Pt(L1)_2$]$^-$), 632.1 ([$Na_3Pt(L1)_2$ –CO_2]$^-$), 326.3 ([$Na_2Pt(L1)_2$]$^{2-}$).

$Na_4[CuL1)_2]$ (**17-Na**):[16] Compound **17-Na** was prepared similarly as described for **14-Na** by reaction of $[Cu(H_2L1)_2]$ (**7**; 1.0 mmol, 480 mg) with NaOH (4.2 ml, 1.0 mol/L, 4.2 mmol), in water (20 ml). Yield: 417 mg (73 % based on anhydrous **17-Na**). Brown powder, very soluble in water and insoluble in acetone, T_{Dec} = 279 °C. EA calcd. for $C_{10}H_8CuN_2Na_4O_8S_4$ (M = 567.93 g/mol): C 21.15, H 1.42, N 4.93 %; found: C 20.79, H 1.42, N 4.74 %. ESI(+)-MS: *m/z* 589.8 ([$Na_5Cu(L1)_2$]$^+$), 567.9 ([$Na_4Cu(L1)(HL1)$]$^+$). ESI(−)-MS: *m/z* 543.7 ([$Na_3Cu(L1)_2$]$^-$), 500.0 ([$Na_3Cu(L1)_2$ –CO_2]$^-$), 260.4 ([$Na_2Pt(L1)_2$]$^{2-}$), 251.9 ([$NaPt(L1)(HL1)$]$^{2-}$). Allowing an aqueous reaction solution to slowly evaporate at r.t. to dryness afforded brown, needle-like single crystals of **17-Na** ·9 H_2O suitable for X-ray structural analysis. Brown, needle-like single crystals of **17-Li** ·*n* H_2O were obtained similarly by using LiOH instead of NaOH during synthesis.

$K_2[Cu(HL1)_2]$ (**17′-K**): Compound **17′-K** was prepared similarly as described for **14′-K** by reaction of $[Cu(H_2L1)_2]$ (**7**; 1.0 mmol, 480 mg) with KOH (2.0 ml, 1.0 mol/L, 2.0 mmol), in water (18 ml). Yield: 219 mg (39 % based on anhydrous **17′-K**). Orange-brown powder, sparingly soluble in water and insoluble in organic solvents, T_{Dec} = 213 °C. EA calcd. for $C_{10}H_{10}CuK_2N_2O_8S_4$ (M = 556.18 g/mol): C 21.60,

H 1.81, N 5.04%; found: C 21.78, H 1.78, N 5.33%. ESI(−)-MS: *m/z* 515.8 ($[KCu(HL1)_2]^-$), 477.7 ($[Cu(HL1)(H_2L1)]^-$), 238.4 ($[Cu(HL1)_2]^{2-}$). Brown, plank-like single crystals of anhydrous **17′-K** suitable for X-ray structural analysis were obtained directly from the mother liquor after standing at r.t. for several days.

$Na_2[Ni(L2)_2]$ (**18-Na**): Upon addition of NaOH solution (2.1 ml, 1.0 mol/L, 2.1 mmol), a suspension of $[Ni(HL2)_2]$ (**8**; 1.0 mmol, 439 mg) in water (20 ml) turned into a clear solution within four hours. Acetone (50 ml) was added under stirring, and the mixture was subsequently stored at −25 °C for 72 h. The crystallized product was isolated by vacuum filtration over a P3 frit, washed with acetone, and dried in air. Yield: 293 mg (47% based on **18-Na** ·8 H_2O). Olive-green, microcrystalline solid, very soluble in water and insoluble in acetone, T_{Dec} = 298 °C. EA calcd. for $C_{12}H_{30}N_2Na_2NiO_{12}S_4$ (*M* = 627.29 g/mol): C 22.98, H 4.82, N 4.47%; found: C 23.15, H 4.59, N 4.41%. ^{1}H NMR (D_2O): δ 2.06 (br, 3H; 3-CH_2 and 4-CH_2), 2.38 (br, 1H; 3-CH_2), 3.73 (br, 2H; 5-CH_2), 4.45 (br, 1H; 2-C*H*) ppm. ^{13}C NMR (D_2O): δ 22.9 (4-CH_2), 30.1 (3-CH_2), 50.4 (5-CH_2), 64.8 (2-*C*H), 177.1 (*C*OO$^-$), 200.3 (*C*SS) ppm. ^{23}Na NMR (D_2O): δ 0.2 ppm. ESI(+)-MS: *m/z* 483.0 ($[Na_2Ni(L2)(HL2)]^+$), 461.0 ($[NaNi(HL2)_2]^+$). ESI(−)-MS: *m/z* 459.9 ($[NaNi(L2)_2]^-$), 436.9 ([Ni-(L2)(HL2)]$^-$), 393.0 ([Ni(L2)(HL2) –CO_2]$^-$). Allowing an aqueous reaction solution to slowly evaporate at r.t. afforded single crystals of **18-Na** ·*n* H_2O suitable for X-ray structural analysis. Identical crystals were obtained by layering an aqueous solution with the threefold volume of acetone under an inert atmosphere of nitrogen. Crystals of hydrated **18-K**, **19-K**, and **20-K** were obtained in a similar manner directly from the respective reaction solutions for **8**/KOH, **9**/KOH, or **10**/KOH.

$Na_2[Ni(L3)_2]$ (**21-Na**): Upon addition of NaOH solution (2.1 ml, 1.0 mol/L, 2.1 mmol), a suspension of $[Ni(HL3)_2]$ (**11**; 1.0 mmol, 539 mg) in water (10 ml) turned into a clear solution within four hours. The solution was evaporated almost to dryness on a rotary evaporator at 40 °C, and subsequently acetone (50 ml) was added. After stirring at r.t. for one hour, the precipitated solid was isolated by vacuum filtration over a P4 frit, washed with acetone, and dried in air. Yield: 611 mg (92% based on **21-Na** ·4.5 H_2O). Yellowish-green powder, soluble in methanol and virtually insoluble in water, insoluble in acetone, T_{Dec} = 290 °C. EA calcd. for $C_{20}H_{27}N_2Na_2NiO_{8.5}S_4$ (*M* = 664.35 g/mol): C 36.16, H 4.10, N 4.22%; found: C 36.24, H 3.80, N 4.14%. ^{1}H NMR (MeOH-D_4): 3.97 (2H; CH_2COO), 4.91 (2H; CH_2Ph), 7.29–7.40 (m, 5H; C*H* Ph) ppm. ^{13}C NMR (MeOH-D_4): δ 51.5 (*C*H_2COO), 53.5 (*C*H_2Ph), 129.2 (*p*-*C*H Ph), 129.5 (*o*-*C*H Ph), 129.9 (*m*-*C*H Ph), 136.0 (*i*-*C* Ph), 172.9 (*C*OO), 209.9 (*C*SS) ppm. ^{23}Na NMR (MeOH-D_4): δ −2.8 ppm. ESI(+)-MS: *m/z* 583.1 ($[Na_2Ni(L3)(HL3)]^+$), 561.0 ($[NaNi(HL3)_2]^+$). ESI(−)-MS: *m/z* 558,8 ($[NaNi(L3)_2]^-$), 536.8 ([Ni(L3)(HL3)]$^-$), 493.0 ([Ni(L3)(HL3) –CO_2]$^-$). Allowing a solution in water/ethanol (1 : 1) to slowly evaporate at r.t. afforded single crystals of **21-Na** ·4.5 H_2O suitable for X-ray structural analysis. Single crystals of **22-Na** ·4.5 H_2O were obtained similarly.

Acknowledgements

This work is supported by the German Research Foundation (DFG), project number 462687456 (https://gepris.dfg.de/ gepris/projekt/462687456). General financial support of the Otto von Guericke University Magdeburg and the Friedrich Schiller University Jena is gratefully acknowledged. Open Access funding enabled and organized by Projekt DEAL.

Conflict of Interest

The authors declare no conflict of interest.

Data Availability Statement

The data that support the findings of this study are available in the supplementary material of this article.

Keywords: Amino acids · Crystal structure · Coordination polymers · Heterobimetallic · Sulfur ligands

[1] a) S. H. Crook, B. E. Mann, A. J. H. M. Meijer, H. Adams, P. Sawle, D. Scapens, R. Motterlini, *Dalton Trans.* **2011**, *40*, 4230; b) T. Zhang, M. Li, Y. Gong, N. Xi, Y. Zheng, Q. Zhao, Y. Chen, B. Liu, *J. Biol. Inorg. Chem.* **2016**, *21*, 807; c) L. Wu, X. Cai, H. Zhu, J. Li, D. Shi, D. Su, D. Yue, Z. Gu, *Adv. Funct. Mater.* **2018**, *28*, 1804324; d) X. Wang, B. Gao, G. S. A. Suleiman, X. Ren, J. Guo, S. Xia, W. Zhang, Y. Feng, *Chem. Eng. J.* **2021**, *424*, 130430; e) R. A. Motterlini, B. E. Mann, D. A. Scapens, *WO* **2008**/003953 A2.

[2] a) R. Pasqualini, E. Bellande, V. Comazzi, J. Laine, *WO* **1993**/01839, **1993**; b) M. A. Stalteri, S. J. Parrott, V. A. Griffiths, J. R. Dilworth, S. J. Mather, *Nucl. Med. Commun.* **1997**, *18*, 870; c) M. Liu, X. Lin, X. Song, Y. Cui, P. Li, X. Wang, J. Zhang, *J. Radioanal. Nucl. Chem.* **2013**, *298*, 1659; d) Y. Chen, H. Guo, F. Xie, J. Lu, *J. Labelled Compd. Radiopharm.* **2014**, *57*, 12.

[3] a) S. Fujii, Y. Suzuki, T. Yoshimura, H. Kamada, *Am. J. Physiol.* **1998**, *247*, G857–G862; b) H. Nakagawa, N. Ikota, T. Ozawa, *Biochem. Mol. Biol. Int.* **1998**, *45*, 1129; c) S. Pou, P. Tsai, S. Porasuphatana, H. J. Halpern, G. V. R. Chandramouli, E. D. Barth, G. M. Rosen, *Biochim. Biophys. Acta* **1999**, *1427*, 216; d) T. Ozawa, N. Ikota, H. Nakagawa, JP2000128893, **2000**; e) S. Fujii, K. Kobayashi, S. Tagawa, T. Yoshimura, *J. Chem. Soc. Dalton Trans.* **2000**, 3310; f) C. A. Davies, P. G. Winyard, WO2002016934, **2002**; g) H. Yasui, S. Fujii, T. Yoshimura, H. Sakurai, *Free Radical Res.* **2004**, *38*, 1061.

[4] L. Sindellari, L. Trincia, M. Nicolini, M. Carrara, S. Zampiron, *Inorg. Chim. Acta* **1987**, *137*, 109.

[5] a) G. Faraglia, D. Fregona, S. Sitran, L. Giovagnini, C. Marzano, F. Baccichetti, U. Casellato, R. Graziani, *J. Inorg. Biochem.* **2001**, *83*, 31; b) A. Trevisan, C. Marzano, P. Cristofori, M. B. Venturini, L. Giovagnini, D. Fregona, *Arch. Toxicol.* **2002**, *76*, 262; c) V. Alverdi, L. Giovagnini, C. Marzano, R. Seraglia, F. Bettio, S. Sitran, R. Graziani, D. Fregona, *J. Inorg. Biochem.* **2004**, *98*, 1117; d) C. Marzano, F. Bettio, F. Baccichetti, A. Trevisan, L. Giovagnini, D. Fregona, *Chem.-Biol. Interact.* **2004**, *148*, 37; e) D. Aldinucci, L. Cattaruzza, D. Lorenzon, L. Giovagnini, D. Fregona, A. Colombatti, *Oncol. Res.* **2008**, *17*, 103; f) R. Verron, T. Achard, C. Seguin, S. Fournel, S. Bellemin-Laponnaz, *Eur. J. Inorg. Chem.* **2020**, 2552.

[6] L. Giovagnini, L. Ronconi, D. Aldinucci, D. Lorenzon, S. Sitran, D. Fregona, *J. Med. Chem.* **2005**, *48*, 1588.

[7] a) L. Giovagnini, S. Sitran, M. Montopoli, L. Caparrotta, M. Corsini, C. Rosani, P. Zanello, Q. P. Dou, D. Fregona, *Inorg. Chem.* **2008**, *47*, 6336; b) R. Cao, R. Villalonga, A. M. Díaz-García, T. Rojo, M. C. Rodríguez-Argüelles, *Inorg. Chem.* **2011**, *50*, 4705; c) C. Nardon, D. Fregona, WO **2018**/100560, A1.

[8] C. Nardon, D. Fregona, L. Brustolin, N. Pettenuzzo, *WO* **2018**, 100561 A1, .

[9] L. Brustolin, C. Nardon, N. Pettenuzzo, N. Zuin Fantoni, S. Quarta, F. Chiara, A. Gambalunga, A. Trevisan, L. Marchiò, P. Pontisso et al., *Dalton Trans.* **2018**, *47*, 15477.
[10] C. Chen, K.-W. Yang, Le Zhai, H.-H. Ding, J.-Z. Chigan, *Bioorg. Chem.* **2022**, *118*, 105474.
[11] A. M. Díaz, R. Villalonga, R. Cao, *J. Coord. Chem.* **2009**, *62*, 100.
[12] a) L. Ronconi, L. Giovagnini, C. Marzano, F. Bettìo, R. Graziani, G. Pilloni, D. Fregona, *Inorg. Chem.* **2005**, *44*, 1867; b) D. Aldinucci, D. Lorenzon, L. Stefani, L. Giovagnini, A. Colombatti, D. Fregona, *Anti-Cancer Drugs* **2007**, *18*, 323; c) D. Fregona, C. Marzano, L. Ronconi, IT1347835, **2003**; d) C. Marzano, L. Ronconi, F. Chiara, M. C. Giron, I. Faustinelli, P. Cristofori, A. Trevisan, D. Fregona, *Int. J. Cancer* **2011**, *129*, 487; e) C. Nardon, G. Boscutti, C. Gabbiani, L. Massai, N. Pettenuzzo, A. Fassina, L. Messori, D. Fregona, *Eur. J. Inorg. Chem.* **2017**, 1737; f) G. Boscutti, C. Nardon, L. Marchiò, M. Crisma, B. Biondi, D. Dalzoppo, L. Dalla Via, F. Formaggio, A. Casini, D. Fregona, *ChemMedChem* **2018**, *13*, 1131; g) A. K. Hartmann, S. Gudipati, A. Pettenuzzo, L. Ronconi, J. L. Rouge, *Bioconjugate Chem.* **2020**, *31*, 1063.
[13] S. Wajda, K. Drabent, *Bull. Acad. Pol. Sci. Ser. Sci. Chim.* **1977**, *25*, 655.
[14] S. Wajda, K. Drabent, *Bull. Acad. Pol. Sci. Ser. Sci. Chim.* **1977**, *25*, 963.
[15] T.-C. Woon, M. J. O'Connor, *Ast. J. Chem.* **1981**, *34*, 2039.
[16] K. Vanthoeun, T. Bunho, R. Mitsuhashi, T. Suzuki, M. Kita, *Inorg. Chim. Acta* **2013**, *394*, 410.
[17] Z. Leka, D. Vojta, M. Kosović, N. Latinović, M. Đaković, A. Višnjevac, *Polyhedron* **2014**, *80*, 233.
[18] W. Beck, M. Girnth, M. Castillo, H. Zippel, *Chem. Ber.* **1978**, *111*, 1246.
[19] M. Castillo, J. J. Criado, B. Macias, M. V. Vaquero, *Inorg. Chim. Acta* **1986**, *124*, 127.
[20] M. Castillo, J. J. Criado, B. Macías, M. V. Vaquero, *Transition Met. Chem.* **1986**, *11*, 476.
[21] Z. B. Leka, V. M. Leovac, S. Lukić, T. J. Sabo, S. R. Trifunović, K. M. Szécsényi, *J. Therm. Anal. Calorim.* **2006**, *83*, 687.
[22] J. J. Criado, I. Fernandez, B. Macias, J. M. Salas, M. Medarde, *Inorg. Chim. Acta* **1990**, *174*, 67.
[23] J. J. Criado, A. Carrasco, B. Macias, J. M. Salas, M. Medarde, M. Castillo, *Inorg. Chim. Acta* **1989**, *160*, 37.
[24] P. Liebing, J. Witzorke, F. Oehler, M. Schmeide, *Inorg. Chem.* **2020**, *59*, 2825.
[25] V. Behling, B. Kintzel, J. Heinrich, M. Hingel, J. Meyer, S. Greiner, P. Liebing, *Cryst. Growth Des.* **2023**, *23*, 7777.
[26] L. Ronconi, C. Maccato, D. Barreca, R. Saini, M. Zancato, D. Fregona, *Polyhedron* **2005**, *24*, 521.
[27] M. P. Kasalović, A. Petrović, J. M. Živković, L. Kuckling, V. V. Jevtić, J. Bogojeski, Z. B. Leka, S. R. Trifunović, N. Đ. Pantelić, *J. Mol. Struct.* **2021**, *1229*, 129622.
[28] P. Liebing, F. Oehler, J. Witzorke, *Crystals* **2020**, *10*, 505.
[29] P. Liebing, F. Oehler, J. Witzorke, M. Schmeide, *CrystEngComm* **2020**, *22*, 7838.
[30] a) Y. Arafat, S. Ali, S. Shahzadi, M. Shahid, *Bioinorg. Chem. Appl.* **2013**, 351262; b) A. Abbas, S. Ali, S. Shahzadi, S. K. Sharma, K. Qanungo, *Russ. J. Gen. Chem.* **2015**, *85*, 1725.
[31] a) S. Hussain, I. H. Bukhari, S. Ali, S. Shahzadi, M. Shahid, K. S. Munawar, *J. Coord. Chem.* **2015**, *68*, 662; b) J. Fatima, S. Hussain, S. Ali, S. Shahzadi, S. Ramzan, M. Shahid, *Russ. J. Gen. Chem.* **2016**, *86*, 2914; c) S. Hussain, S. Ali, S. Shahzadi, M. Shahid, A. A. Tahir, S. M. Abbas, M. Riaz, I. Ahmad, I. Hussain, *J. Coord. Chem.* **2017**, *70*, 4070.
[32] C. R. Groom, I. J. Bruno, M. P. Lightfoot, S. C. Ward, *Acta Crystallogr.* **2016**, *B72*, 171.
[33] P. Patnaik, *Handbook of inorganic chemicals*, McGraw-Hill, New York, **2003**.
[34] a) Y. Huang, Y.-H. Tsai, W.-C. Hung, C.-S. Lin, W. Wang, J.-H. Huang, S. Dutta, C.-C. Lin, *Inorg. Chem.* **2010**, *49*, 9416; b) W.-Y. Lu, H.-W. Ou, C.-N. Lee, J. K. Vandavasi, H.-Y. Chen, C.-C. Lin, *Polymer* **2018**, *139*, 1.
[35] J. F. Kögel, E. Lork, M. Lõkov, E. Parman, I. Leito, A. Y. Timoshkin, J. Beckmann, *Eur. J. Inorg. Chem.* **2019**.
[36] M. J. McGeary, K. Folting, W. E. Streib, J. C. Huffman, K. G. Caulton, *Polyhedron* **1991**, *10*.
[37] A. Bondi, *J. Phys. Chem.* **1964**, *68*, 441.
[38] R. L. Davidovich, A. V. Gerasimenko, V. B. Logvinova, S.-Z. Hu, *Zh. Neorg. Khim.* **2003**, *48*, 69.
[39] M. Font-Bardia, X. Solans, M. Font-Altaba, *Acta Crystallogr.* **1993**, *C49*, 1452.
[40] M. K. Krawczyk, T. Lis, *Acta Crystallogr.* **2011**, *C67*, m266–74.
[41] G. M. Sheldrick, *Acta Crystallogr.* **2015**, *A71*, 3.
[42] G. M. Sheldrick, *Acta Crystallogr.* **2015**, *C71*, 3.
[43] O. V. Dolomanov, L. J. Bourhis, R. J. Gildea, J. A. K. Howard, H. Puschmann, *J. Appl. Crystallogr.* **2009**, *42*, 339.
[44] M. Pinsky, D. Avnir, *Inorg. Chem.* **1998**, *37*, 5575.
[45] P. Liebing, J. Heinrich, J. Witzorke, M. Kühling, S. Busse, C. Swanson, *Chem. Select* **2021**, *6*, 11729.

Manuscript received: May 5, 2024
Revised manuscript received: July 31, 2024
Accepted manuscript online: August 9, 2024

